SI Appendix for: Unraveling the disease consequences and mechanisms of modular structure in animal social networks

Sah et al. 10.1073/pnas.1613616114

SI Materials and Methods

Animal social networks. We obtained previously published (and publicly available) social networks of 69 groups across 43 animal species. The networks were selected based on the criterion that edge connections can serve as actual routes of infectious disease spread. For groups that had multiple temporal snapshots of social network, we randomly selected one network for the analysis to avoid intra-group correlation in network metrics. Few networks had weighted edges. To enable consistent comparison across all networks, we transformed the edges of these networks to binary edges by employing an edge filtering approach (1). To this end, edges with weights less than 50^{th} percentile of edge weights were removed from the network, and the remaining edges were assigned an edge weight of one.

Measure of relative modularity. We used modularity (Q) proposed by Newman (2, 3) to measure the strength of modular organization in networks. Modularity can be defined as:

$$Q = \sum_{k=1}^{K} (e_{kk} - a_k^2) \quad [1]$$

where e_{kk} denotes the fraction of edges within the subgroup k and a_k is the fraction of the total edges present within the subgroup. If $\overline{d^k}$ is the average degree of individuals in subgroup k, $\overline{d_w^k}$ is the average within subgroup degree and s_k is the total number of individuals in the subgroup, then the equation 1 can be rewritten as:

$$Q = \sum_{k=1}^{K} \left[\frac{\overline{d_w^k} s_k}{\overline{d} n} - \left(\frac{\overline{d^k} s_k}{\overline{d} n} \right)^2 \right] \quad [2]$$

where $\overline{d}$ is the average degree of the network, and the total number of individuals and subgroups in the network are n and K, respectively.

Let L_k be the total edges of individuals of a subgroup k out of which L_k^w are the edges present within the subgroup. Equation (2) can then be further reduced to:

$$Q = \sum_{k=1}^{K} \left[\frac{L_k^w}{L} - \left(\frac{L_k}{L} \right)^2 \right] \quad [3]$$

where L is the total edges present in the network.

We estimated Newman modularity, Q, for the largest connected component of each animal social network using the Louvain method as described in (4).

The highest possible modularity in a network is achieved when all individuals in a subgroup k only interact with each other and no edges are present between subgroups (i.e., subgroups are disjointed). In other words, $Qmax$ of a network is when $L_k^w = L_k$. Equation S3 can be therefore written as

$$Q_{max} = \sum_{k=1}^{K} \left[\frac{L_k}{L} - \left(\frac{L_k}{L} \right)^2 \right] \quad [4]$$

A network is more modular if its observed Q value is closer to the maximum possible modularity. We thus normalize the strength of modular organization with respect to its Q_{max} by computing relative modularity of networks as $Q_{rel} = \frac{Q}{Q_{max}}$.

Mechanisms of modular organization. We test the role of several features of social organization in animal societies that may contribute towards the observed magnitude of relative modularity. These features include network size (n); (log of the) number of subgroups in the social network (network fragmentation); preferential association with own subgroup (subgroup cohesion, measured as the proportion of total contacts that occur within subgroups); variation in subgroup cohesion across the network; average and variation in subgroup sizes; average and variation in number of individual contacts (degree); and variation in contacts among subgroups (subgroup degree variation). We note that this is not an exhaustive list but includes factors that we believe can be important in the context of animal social networks. Average contacts of subgroups was not included in the analysis because mathematically it is equal to the average degree of individuals.

To examine the relative contribution of these factors towards network modularity, we ran the following mixed effects beta regression model using glmmADMB package (version 0.8.3.3) in R (version 3.2.3). All predictors were centered and scaled to unit variances to assign same prior importance to each predictor in the analysis (5). The distributions of network size and number of subgroups were skewed to the right and therefore were natural log-transformed for further analyses. For all the variance predictors, we estimated coefficient of variation ($CV = \sigma/\mu$) to avoid possible correlation with their average predictor counterparts. To avoid multicollinearity, we estimated the variance inflation factor (VIF) implemented in the package 'car' in R, and removed predictors with VIF >5 (6). We treated the species nested within the order of the social group and sociality as random effects in the model.

Generation of null networks. Two types of null networks were generated for each animal social network. *Modular null networks* were created in two steps: first, within-subgroup connections were randomized and the second step involved randomization of between-subgroup connections. Edges were randomized using the double-edge swap operation in the NetworkX package (7). The modular null networks, therefore, had the same modular subdivision and degree sequence as the empirical networks, but were random with respect to other higher-order network properties. We generated *homogeneous null networks* by performing simultaneous edge swaps over

within- and between-subgroup connections, which preserves the local contact heterogeneity but randomizes all higher-order features of the network including network modularity (8).

Generation of synthetic modular networks. We generated synthetic modular networks using modular random network generator described in (8). This model allows generation of modular networks by varying the level of network fragmentation or subgroup cohesion while keeping other network properties (such as degree homophily, clustering coefficient) close to homogeneous null network with no modular structure. In this study we generated modular networks with 10,000 nodes. The strength of modular organization was varied by adjusting either subgroup cohesion or network fragmentation. As the total number of individuals was fixed across all generated synthetic networks, increasing network fragmentation (i.e., the number of subgroups) also coincided with decreasing the average subgroup size in the network. Unless otherwise noted, we assumed local contact heterogeneity in social groups to follow an exponential degree distribution with mean contact (degree) of 10.

Disease simulations. We performed Monte-Carlo simulations of discrete-time susceptible-infected-recovered (SIR) model of disease spread. Each disease simulation was initiated by infecting a randomly chosen individual in the social group. At subsequent time steps every infected individual(s) in the population could either transmit infection to a susceptible neighbor with probability parameter β or recover with probability parameter γ. The disease simulation was terminated when there were no remaining infected nodes in the network. As we were interested only in major outbreaks, we considered only those simulations in our calculations where at least 10% individuals in the network acquired infection. Pathogen contagiousness was measured in terms of infection transmissibility. Transmissibility was defined as the probability of pathogen transmission from an infected to susceptible host during the period when the host is infectious. Assuming the individual's recovery and infection transmission to be a Poisson process, transmissibility was calculated as: $T = \frac{\beta}{\beta+\gamma}$.

Disease simulations in Figure 2C and 5: To compare epidemiological consequences of empirical networks, we simulated infectious disease spread with basic reproduction number, $R_0 = 1.2$. Basic reproduction number is defined as the average number of secondary infections caused by a single infected host in a completely susceptible population. Following ref. (9), we estimate transmissibility of pathogen corresponding as:

$$T = R_0\left(\frac{\langle k\rangle}{\langle k^2\rangle - \langle k\rangle}\right) \qquad [5]$$

where $\langle k\rangle$ and $\langle k^2\rangle$ are the mean degree and mean square degree of the networks, respectively. Since empirical networks had varying values of $\langle k\rangle$ and $\langle k^2\rangle$, we obtained a different value of pathogen transmissibility corresponding to a $R_0 = 1.2$ for each empirical network. For consistent comparison, disease simulations on null networks were performed using the same value of pathogen transmissibility that was estimated for their empirical network counterpart using equation 5.

Threshold analysis. We identified the threshold of pathogen contagiousness below which there is a minimal risk of large outbreak in modular networks using the formula proposed in ref. (10). Specifically, the threshold is estimated numerically as:

$$\Delta = \frac{\sqrt{\langle\rho^2\rangle - \langle\rho\rangle^2}}{\langle\rho\rangle} \qquad [6]$$

where ρ denotes the outbreak sizes of Monte-Carlo disease simulations, and Δ is a variability measure. The epidemic threshold is estimated by performing disease simulations over a wide range of pathogen transmissibility and estimating the corresponding Δ measure. The pathogen transmissibility where Δ peaks is considered to be the epidemic threshold (10).

Table S1. Multivariable analysis on determinants of modular organization in the dynamic networks of four species (*C. fellah*, *C. pennsylvanicus*, *P. lotor*, and *M. agrestis*)

Explanatory variable	Effect size	95% confidence intervals
Intercept	0.05	0.03 – 0.07
Network size	-0.03	-0.05 – 0.00
Network fragmentation*	**0.48**	**0.44 – 0.52**
Subgroup cohesion*	**0.87**	**0.85 – 0.90**
Subgroup cohesion variation	–	–
Subgroup size average	–	–
Subgroup size variation*	**-0.10**	**-0.12 – -0.08**
Individual degree average	–	–
Individual degree variation	-0.02	-0.06 – 0.02
Subgroup degree variation*	**-0.04**	**-0.07 – -0.02**
Random effects	**Variance estimate (σ^2)**	
Group identification	0.0002	

Response variable is the relative modularity, Q_{rel}, of the social networks. Asterisks and bold text indicate significance. We treated the social group identity of each network as the random effect. Explanatory variables with VIF>5 were dropped from the model, and therefore their effect sizes therefore were not estimated.

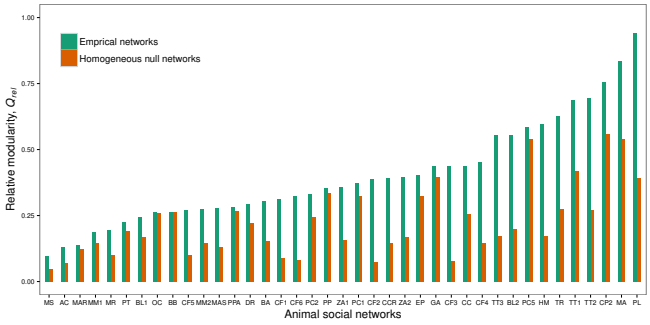

Fig. S1. Empirical animal social networks and the corresponding *homogeneous null networks* included in Fig.2*C*. Animal social network abbreviations: AC = *Acanthiza* spp., CC = *Cercopithecus campbelli*, CCR = *Crocuta crocuta*, CF = *Camponotus fellah*, CP = *Camponotus pennsylvanicus*, BB= *Bison bison*, BL = *Branta leucopsis*, EP = *Erythrocebus patas*, GA = *Gasterosteus aculeatus*, HM = *Haemorhous mexicanus*, MA = *Mirounga angustirostris*, MAR = *Macaca arctoides* , MM = *Macaca mulatta*, MS = *Myotis sodalis*, OC = *Ovis canadensis*, PC = *Papio cynocephalus* , PL = *Procyon lotor*, PP = *Pan paniscus*, PT = *Pan troglodytes*, TR = *Tiliqua rugosa*, TT = *Tursiops truncatus*, ZA = *Zonotrichia atricapilla*. Numbers next to the species acronym indicate a separate social group.

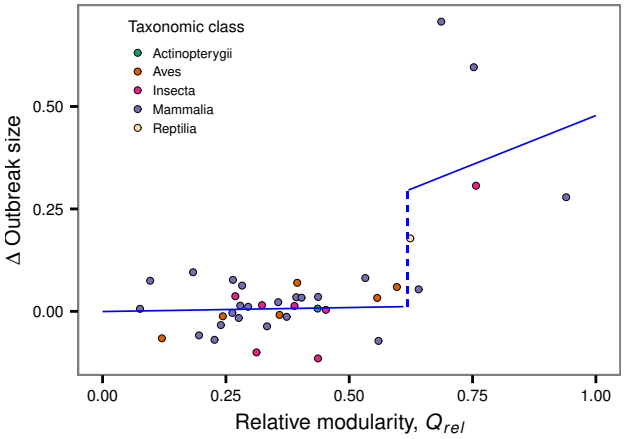

Fig. S2. Threshold value of relative modularity above which the empirical networks tend to experience lower outbreak sizes as compared to homogeneous null networks in Fig.2*C*. The breakpoint is at $Q_{rel} \approx 0.618$. Δ Outbreak size is the relative outbreak size and is calculated as $\frac{S_{null}-S_{emp}}{S_{emp}}$ where S = average outbreak size, emp = empirical network, $null$ = homogeneous null networks. We recursively fit a piecewise linear mixed regression model with a sequence of increasing breakpoint values. The optimum breakpoint value was selected from the model with minimum deviance. To take into account any correlation within the taxonomic groups, we used the species nested with genus and taxonomic order of the groups as a random effect in the model. Sociality of the animal groups analyzed (relative solitary, social, and fission-fusion) was also included as a random effect.

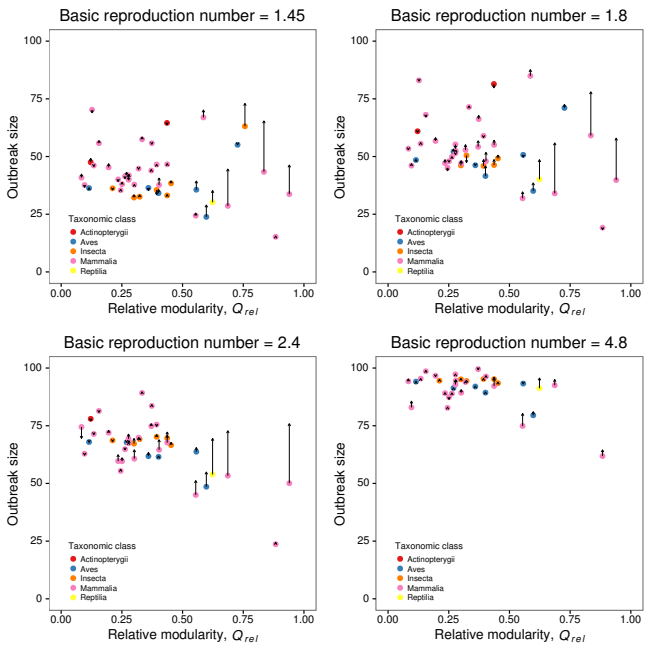

Fig. S3. *Extended figure of Fig.2C* Comparisons between real (filled points) and their homogeneous null networks (tip of arrows) with respect to the percentage of infected individuals (outbreak size) due to an outbreak with basic reproduction number, R_0 equal to 1.45, 1.8, 2.4 and 4.8. Point color corresponds to the taxonomic class of the animal group. Social networks with non-significant modular subdivision (as indicated by *t* test analysis) have been excluded. The generated homogeneous null networks preserve only the local heterogeneity of contacts among individuals; the arrows therefore indicate the change in direction and magnitude of outbreak size under the scenario where all higher-order structural complexities (including modular subdivisions) are removed from animal social networks.

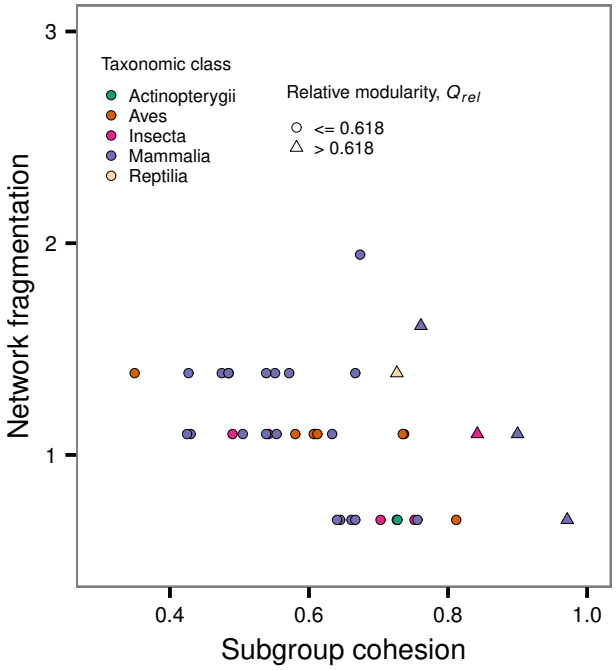

Fig. S4. The values of network fragmentation and subgroup cohesion present in empirical animal social networks. Network fragmentation is the log-transformed value of the total subgroups present in the social network. Circles are the networks with Q_{rel} <0.618 (the threshold value shown in Fig.2c of the main text and SI Appendix, Fig.S2) and triangles represent social networks above the modularity threshold. Animal social networks above the threshold experienced lower outbreak size as compared to homogeneous null networks in Fig.2*C*. In this study, we show that the disease consequences of modular subdivision in animal social networks are driven by network fragmentation and subgroup cohesion.

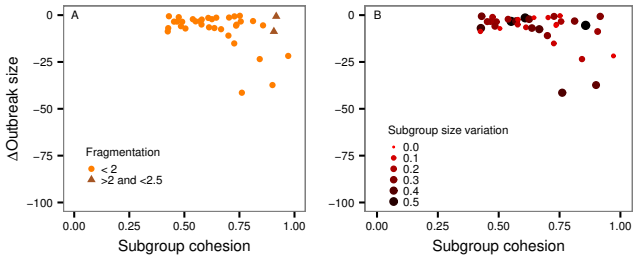

Fig. S5. Reduction in outbreak size experienced by empirical animal social networks as compared to their homogeneous null networks (as shown in Fig.2*C*) as a function of subgroup cohesion and (A) network fragmentation, and (B) subgroup size variation.

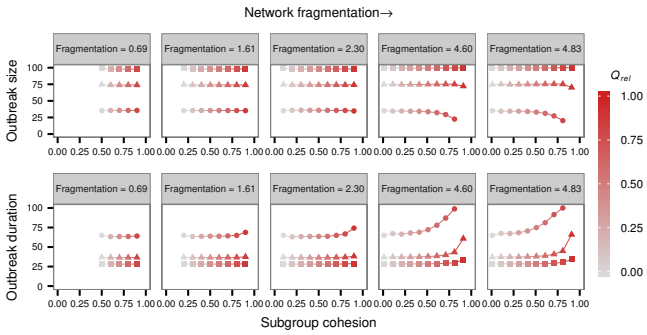

Fig. S6. *Extended figure of Fig.3D.* Disease implications of modular subdivisions in synthetic modular networks as a function of subgroup cohesion and network fragmentation. Outbreak size and duration have been normalized to the maximum observed outbreak size and duration respectively. Subgroup cohesion measures the tendency of individuals to interaction with members of their own subgroup, and is measured as the proportion of contacts within-subgroups to total contacts across the entire social network. In theory, a social network with two subgroups is considered to have Q_{rel}=0 when the proportion of contacts within subgroups is equal to the proportion of contacts between subgroups (=0.5). The minimum subgroup cohesion realized in a network is therefore a function of the number of subgroups (fragmentation) present in the network. Circles, triangles and squares summarize disease outbreaks of pathogen transmissibility of 0.1, 0.18 and 0.3, respectively.

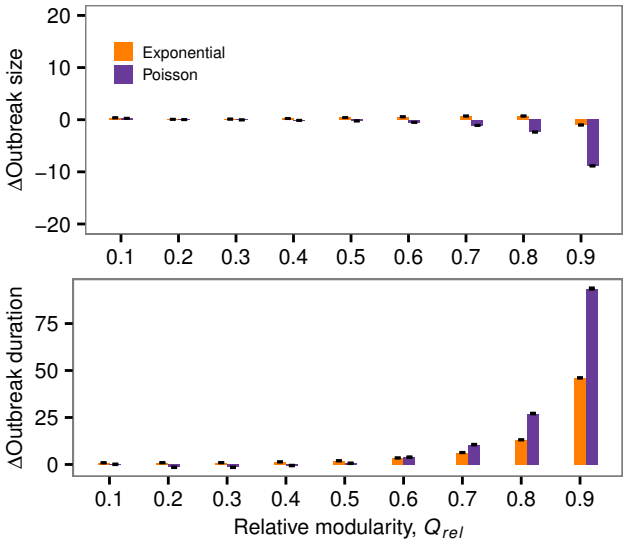

Fig. S8. Disease burden in modular social networks with Poisson (purple bars) and exponential (orange bars) contact heterogeneity. The y-axis measures the change in outbreak size and duration of modular networks as compared to disease burden in homogeneous networks (with Q_{rel}=0), and is calculated as $O_{modular} - O_{non-modular}$, where $O_{modular}$ and $O_{non-modular}$ is the average outbreak size or duration of networks with $Q_{rel} > 0$ and $Q_{rel} = 0$, respectively. Errors bars represent standard error of the means.

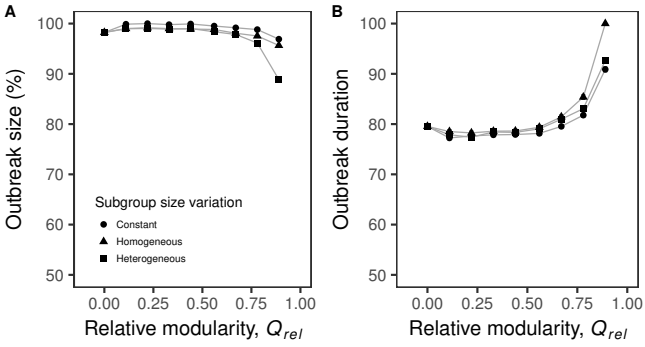

Fig. S7. (A) Outbreak size and (B) outbreak duration in networks with different heterogeneity in subgroup sizes. Constant = all subgroups have equal number of individuals; homogeneous = subgroup size distribution follows a Poisson distribution; heterogeneous = subgroup sizes follow an exponential distribution. For homogeneous and heterogeneous subgroup size distribution, the average subgroup size = N/network fragmentation, where N is total number of individuals in the social group. Results summarize disease simulations of a pathogen with transmissibility = 0.1 over networks with 10 subgroups. Outbreak size and duration have been normalized to the maximum observed outbreak size and duration respectively.

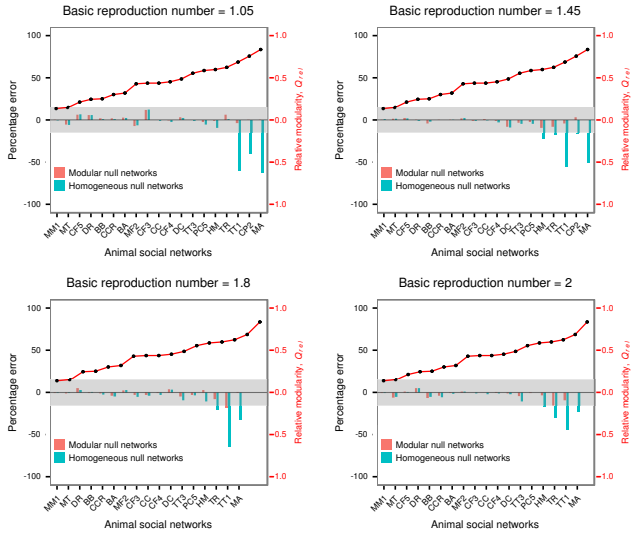

Fig. S9. *Extended figure of Fig.5.* Percentage error in outbreak size predictions using modular and homogeneous null networks for 19 animal social networks due to an outbreak with R_0 = 1.05, 1.45, 1.8 and 2.0. Percentage error is calculated as $(S_{emp} - S_{null})/S_{emp} \times 100$, where S = outbreak size, emp = empirical network, $null$ are modular or homogeneous null networks of the empirical network. The social networks are ordered according to the increasing value of relative modularity (red solid curve, secondary y-axis). The shaded region indicates the range of percentage error values below 15%. BA, *Brachyteles arachnoides*;BB, *Bison bison*; CC, *Cercopithecus campbelli*; CCR, *Crocuta crocuta*; CF, *C. fellah*; CP, *C. pennsylvanicus*; DC, dairy cattle; DR, *Desmodus rotundus*; HM, *Haemorhous mexicanus*; MA, *M. angustirostris*; MF, *Macaca fuscata*; MM, *Macaca mulatta*; MT, *Macaca tonkeana*; PC, *Papio cynocephalus*; TR, *T. rugosa*; TT, *T. truncates*. Numbers denote separate groups of the same species.

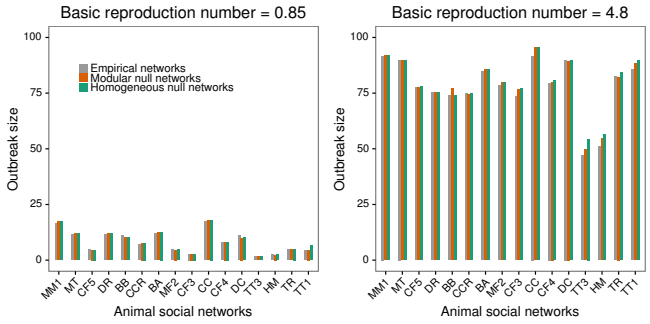

Fig. S10. Outbreak size predictions from modular and homogeneous null networks as compared to the "true" outbreak size (empirical networks, gray vertical bars). Results are shown for simulations of a slowly (R_0=0.85) and rapidly (R_0=4.8) spreading infectious disease. Outbreak size is averaged across all disease simulations. Both the null networks (in most cases) yield identical and accurate outbreak size predictions.

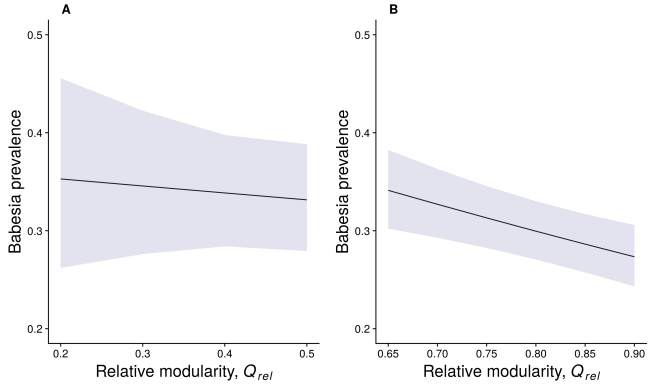

Fig. S11. Highly modular networks are able to reduce outbreak size. Empirical evidence from the spread of *Babesia* parasite in the field voles (*Microtus agrestis*): *Babesia* are spread by ticks and therefore networks based on common space use are appropriate to model the parasite transmission (11, 12). We therefore used the bipartite networks described in (13) to examine the relationship between network modularity and parasite transmission. Specifically, generalized linear mixed model with binomial response distribution was used, where *Babesia* prevalence was entered as the response and the relative modularity of networks in the previous sampling period was entered as the explanatory variable (for details see (13)). The number of nodes and the total edges were also entered as explanatory variables in the model to control for variation in the sampling effort. Additionally, the site of data collection was included as a random effect. To control for autocorrelation, we included the parasite prevalence in the previous sampling period as an explanatory variable. Two models were fit - one that explored the relationship between parasite prevalence and relative modularity in networks where $Q_{rel} \leq 0.6$, and other that examined association between parasite prevalence and relative modularity for networks where $Q_{rel} > 0.6$. No significant association was found between network modularity and *Babesia* prevalence when $Q_{rel} \leq 0.6$ (χ^2 = 0.21, P=0.65). However, *Babasia* prevalence decreased with increasing modularity when $Q_{rel} > 0.6$ (χ^2 = 12.50, P < 0.001).

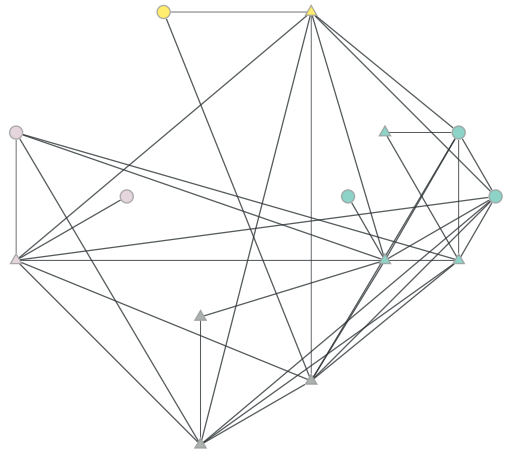

Fig. S12. Low modular networks do not limit global disease transmission. Empirical evidence from the spread of a gastrointestinal parasite in brown spider monkeys (*Ateles hybridus*) (14). Gastrointestinal parasites have been empirically shown to spread through the networks of physical interaction in brown spider monkeys (14). In the social networks of brown spider monkeys described in ref. (14), we identified four connected subgroups with a Q_{rel} of 0.24. Node colors indicate different subgroups. The triangle shaped nodes are the individuals that were reported infected with *Strongyloides sp.* in (14). The parasite prevalence in the connected component of the network was 57%. No structural trapping was observed in the network (i.e., infections were reported in all subgroups), which suggests that the low modularity of spider monkey social network does not inhibit the global spread of parasites.

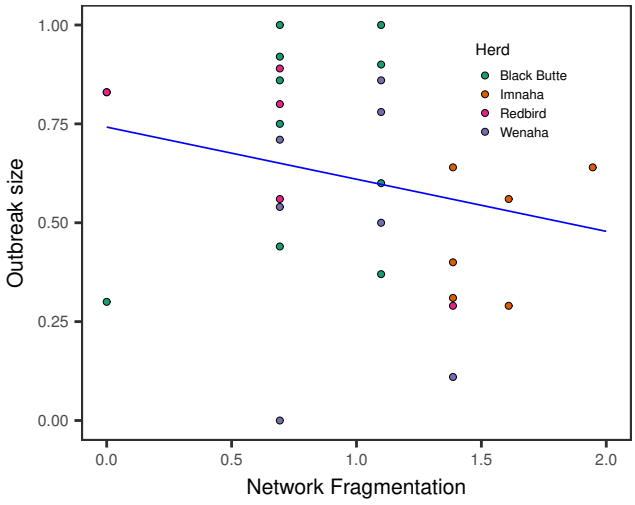

Fig. S13. Structural trapping of infectious disease increases with network fragmentation. Empirical evidence from the spread of pneumonia in the big horn lambs (*Ovis canadensis*). Subgroups in big-horn lambs in (15) were identified based on direct or indirect association between animals to study the spread of pneumonia between individuals. This definition of subgroup implies that between-group interaction was minimal (i.e., high subgroup cohesion). Lamb mortality was considered to be a reasonable proxy of infection status (15); we therefore calculated the outbreak size as the proportion of deaths within each lamb herd (population). In the figure, each population is represented by a different point color. We found negative (albeit weak) relationship between network fragmentation and outbreak size (χ^2 = 3.29, P $= 0.069$).

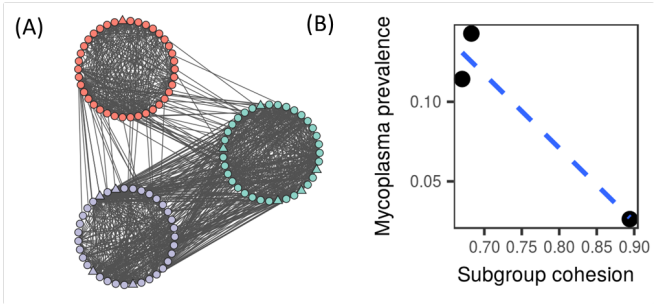

Fig. S14. High subgroup cohesion can induce structural delay of infection spread. Empirical evidence from the spread of *Mycoplasma gallisepticum* in house finches (*Haemorhous mexicanus*) (16). The social network of the songbirds based on common feeder use has been associated with spread of *Mycoplasma gallisepticum* (16). We estimated the relative modularity of the songbird social network to be 0.29 with three connected subgroups. Node colors indicate different subgroups. The triangle shaped nodes are the individuals that were reported infected with *Mycoplasma gallisepticum* in (16). The infection prevalence in the connected component of network was 9%. No structural trapping was observed (i.e., infections were reported in all the subgroups) in the network, which suggests that low modularity does not inhibit global transmission. However, the local disease prevalence (B) was inversely correlated to subgroup cohesion in the interaction networks of songbirds. This suggests that high local (subgroup) cohesion induces structural delay of infection spread within the social network.

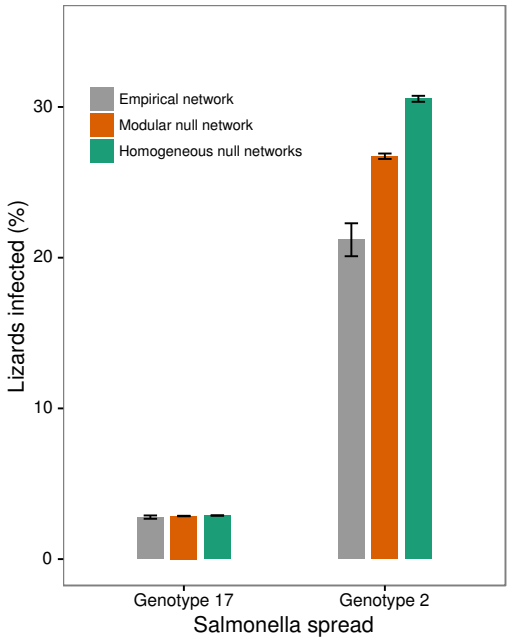

Fig. S15. Modular networks influence disease transmission of moderately, but not low, contagious pathogens/parasites. Networks based on physical proximity are associated with the spread of *Salmonella* in Australian sleepy lizards (17). Our investigation of modular subdivisions in the social network revealed network modularity to be moderately high (Q_{rel} = 0.624). We used the transmission data of two Salmonella strains (published in ref. (17)) to validate our theoretical prediction that network modularity influences disease transmission of moderately, but not of low contagious pathogen. To do so, we first estimated pathogen transmissibility of the two *Salmonella* strains (Genotype 17 and 2) to be 0.043 (R_0 = 0.48) and 0.1788 (R_0 = 2.02), respectively. The estimated transmissibility value was used to perform simulations of *Salmonella* spread in the modular and homogeneous null networks of sleepy lizards. Finally, the outbreak size of disease simulations was compared to the real transmission data of the two genotypes in the sleepy lizard social network. For the low transmissible strain (Genotype 17), we found that the homogeneous and modular null networks produced identical and accurate outbreak size predictions. This suggests that modular subdivision does not influence transmission of low contagious parasites. Conversely, for the moderately transmissible strain (Genotype 2), modular null networks performed better in estimating the true outbreak size as compared to homogeneous null networks, which suggests that modular subdivision does influence the transmission of moderately transmissible parasites.

Table S2. Empirical (or data-driven modeling) evidence that matches the predictions of our study

Key findings of this study	Evidence	Specific findings	Notes	Reference
Structural trapping by highly modular network localizes infection to a small proportion of subgroups	Plague (*Yersinia pestis*) infection in the great gerbil (*Rhombomys opimus*)	Plague spread easily within burrow systems (defined as subpopulations in the study) than between them. Probability that an animal was infectious or recovered was higher if its subpopulation was known to harbour infected animals in the recent past than if there was no evidence of recent infection	Although network modularity was not explicitly calculated, limited movement of gerbil or infected fleas between burrow systems is indicative of a high network modularity	(18)
Structural delay of infection spread	Canine distemper virus outbreak in Greater Yellowstone ecosystem's wolves (*Canis lupus*) and coyotes (*Canis Latrans*)	Low connectivity (indicative of high modularity) between host population increases outbreak duration	Data driven model	(19)
	Epidemic of phocine distemper virus in the North Sea population of harbour seals (*Phoca vitulina*)	When coupling between host patches is weak (indicative of high modularity), higher number of host patches (fragmentation) increases outbreak duration	Data-driven model	(20)
Low levels of modular organization does not structurally trap infection	*Esherichia coli* transmission in wild elephants (*Loxodonta africana*)	No evidence that animals were more likely to be infected with *E. coli* from members of their own subgroup than members of other subgroups	Aggregation of animals in single large groups suggests social networks to be homogeneous (or low modular) during rainy periods. In addition, the authors observe high overlap in home-ranges around water sources, which indicates social networks are not highly modular during non-rainy seasons	(21)
Effect of modular structure on disease transmission depends on pathogen contagiousness	*Cryptosporidium* spread in wild lemurs	Increasing network modularity reduces outbreak size for moderately transmissible pathogen, but not for low and high pathogen transmissibility	Pathogen transmissibility can be derived from Figure 7 based β and γ values. Data-driven model	(22)

1. Croft DP, James R, Krause J (2008) *Exploring Animal Social Networks*. (Princeton University Press).
2. Newman M, Girvan M (2004) Finding and evaluating community structure in networks. *Physical Review E* 69(2):026113.
3. Newman MEJ (2006) Modularity and community structure in networks. *Proceedings of the National Academy of Sciences of the United States of America* 103(23):8577–82.
4. Blondel VD, Guillaume JL, Lambiotte R, Lefebvre E (2008) Fast unfolding of communities in large networks. *Journal of Statistical Mechanics: Theory and Experiment* 2008(10):P10008.
5. Schielzeth H (2010) Simple means to improve the interpretability of regression coefficients. *Methods in Ecology and Evolution* 1:103–113.
6. Montgomery D, Peck E (1982) Introduction to linear regression analysis, 1992.
7. Hagberg Aa, Schult Da, Swart PJ (2008) Exploring network structure, dynamics, and function using NetworkX. *Proceedings of the 7th Python in Science Conference (SciPy2008)* 836:11—-15.
8. Sah P, Singh LO, Clauset A, Bansal S (2014) Exploring community structure in biological networks with random graphs. *BMC bioinformatics* 15:220.
9. Meyers LA (2007) Contact network epidemiology: Bond percolation applied to infectious disease prediction and control. *Bulletin of the American Mathematical Society* 44(1):63–86.
10. Shu P, Wang W, Tang M, Do Y (2015) Numerical identification of epidemic thresholds for susceptible-infected-recovered model on finite-size networks. *Chaos* 25(6).
11. Godfrey SS, Bull CM, James R, Murray K (2009) Network structure and parasite transmission in a group living lizard, the gidgee skink, *Egernia stokesii*. *Behavioral Ecology and Sociobiology* 63(7):1045–1056.
12. Leu ST, Kappeler PM, Bull CM (2010) Refuge sharing network predicts ectoparasite load in a lizard. *Behavioral ecology and sociobiology* 64(9):1495–1503.
13. Davis S, Abbasi B, Shah S, Telfer S, Begon M (2015) Spatial analyses of wildlife contact networks. *Journal of the Royal Society, Interface* 12(102).
14. Rimbach R, et al. (2015) Brown spider monkeys (Ateles hybridus): a model for differentiating the role of social networks and physical contact on parasite transmission dynamics. *Philosophical Transactions of the Royal Society B: Biological Sciences* 370:20140110.
15. Manlove KR, et al. (2014) Costs and benefits of group living with disease: a case study of pneumonia in bighorn lambs (*Ovis canadensis*). *Proceedings of the Royal Society B* 281(November):20142331.
16. Adelman JS, Moyers SC, Farine DR, Hawley DM (2015) Feeder use predicts both acquisition and transmission of a contagious pathogen in a North American songbird. *Proceedings. Biological sciences / The Royal Society* 282(1815):20151429–.
17. Bull CM, Godfrey SS, Gordon DM (2012) Social networks and the spread of Salmonella in a sleepy lizard population. *Molecular Ecology* 21(17):4386–4392.
18. Davis S, et al. (2007) Plague metapopulation dynamics in a natural reservoir: the burrow system as the unit of study. *Epidemiology and infection* 135(05):740–748.
19. Almberg ES, Cross PC, Smith DW (2010) Persistence of canine distemper virus in the Greater Yellowstone Ecosystem's carnivore community. *Ecological Applications* 20(7):2058–2074.
20. Swinton J, Harwood J, Grenfell BT, Gilligan CA (1998) Persistence thresholds for phocine distemper virus infection in harbour seal *Phoca vitulina* metapopulations. *Journal of Animal Ecology* 67(1):54–68.
21. Chiyo PI, et al. (2014) The influence of social structure, habitat, and host traits on the transmission of *Escherichia coli* in wild elephants. *PLoS ONE* 9(4).
22. Springer A, Kappeler PM, Nunn CL (2016) Dynamic vs. static social networks in models of parasite transmission: Predicting *Cryptosporidium* spread in wild lemurs. *Journal of Animal Ecology*.